J Mater Sci (2011) 46:3191–3199
DOI 10.1007/s10853-010-5203-z

Compressive deformation behavior of Al 2024 alloy using 2D and 4D processing maps

Sasi Bhushan Bhimavarapu · Amit Kumar Maheshwari · Deepti Bhargava · Shashi Prakash Narayan

Received: 9 April 2010 / Accepted: 17 December 2010 / Published online: 30 December 2010
© Springer Science+Business Media, LLC 2010

Abstract The hot deformation behavior of Al 2024 was studied by isothermal hot compression tests in the temperature range of 250–500 °C and strain rate range of 10^{-3} to 10^{2} s^{-1} in a computer-controlled 50 kN servo-hydraulic universal testing machine (UTM). The results show that the flow stress of Al 2024 alloy increases with strain rate and decreases after a peak value, indicating dynamic recovery and recrystallization. The processing map exhibits two domains of optimum efficiency for hot deformation at different strains, including the low strain rate domain at 500 °C and between 10^{-2} and 10^{-1} s^{-1} and the high strain rate domain in 250 and 300 °C in the strain rate range of 10^{1} to 10^{2} s^{-1}. An attempt has been made in this article to generate a new hybrid 4D process map which illustrates contours of power dissipation and instability in the 3D space of strain rate, temperature, and strain.

Introduction

Al 2024 is an age-hardenable aluminum alloy, which is widely used in automobile and aerospace industry due to its excellent properties like low density and good damage tolerance [1]. These metallic materials are processed by various secondary processes like forging, drawing, rolling, etc., that are generally conducted at elevated temperatures for different engineering purposes [2]. Such thermo-mechanical processing techniques cause the change in the intrinsic properties like microstructure and flow instability of the alloy. Hence, microstructural evolution is the key to obtain the desired mechanical properties, which can be controlled through proper implication of defined critical processing parameters. It is important, therefore, to determine the changes in the intrinsic properties of the alloys for a set of mechanical applications by setting up a generalized condition in terms of the critically important processing parameters—flow stress (σ), strain (ε), strain rate ($\dot{\varepsilon}$), and temperature (T)—in order to produce defect free and good quality products [3]. Process maps are often used to define the safe deformation zone for producing the proper metallurgical microstructure in a particular alloy by considering the complementary relationship between the rate of visco-plastic heat generated by the deformation and the rate of energy dissipation associated with microstructural mechanisms occurring during deformation. Some "Mathematical Dynamic Material Models" along with a newly proposed "Modified Johnson–Cook material flow model for hot deformation processing" are discussed in [4]. These models relate the important process parameters under the flow condition behavior.

Although process maps are generally a 2D visualization, which shows the efficiency as contours in strain rate and temperature space, they do not show the effect of strain in one visual representation. Advancements in software like Statistica, Sigmapro, and D-plot, etc., allow the plotting of efficiency and instability values in 3D space of temperature, strain rate, and strain, and thus provides a clear visualization and delineation of the deformability parameters as a function of these three processing variables. Such 4D visualizations are generally used in other scientific fields such as biotechnology, microbiology, and forensic sciences, and are being used for the first time to study energy dissipation and instability during metal processing. In this study, a total of 36 samples were deformed to 0.67

S. B. Bhimavarapu · A. K. Maheshwari (✉) · D. Bhargava · S. P. Narayan
Advanced Materials and Processes Research Institute (CSIR), Bhopal 462064, MP, India
e-mail: ampri.amit@gmail.com

Table 1 Flow stress values of Al 2024 alloy deformed at different strain rates and temperatures tabulated for calculating efficiency and instability for generating processing maps

Strain	Strain rate (s^{-1})	Temperature (°C)					
		250	300	350	400	450	500
0.1	0.001	172.6	113.5	75.7	44.8	19.2	9.4
	0.01	195.9	146.3	102.9	58.5	34.9	19.9
	0.1	228.5	175.1	127.9	80.4	61.8	31.7
	1	204	200.9	147.8	122.8	84.3	65
	10	224.6	210.6	172.1	149.5	118.9	90.7
	100	250.8	206.2	177.4	169.9	125.6	93.7
0.2	0.001	158.2	104.4	68.9	39.2	19.2	9.17
	0.01	196.7	138.2	97.1	54.1	35.3	20
	0.1	220.7	167.1	121.3	76.6	58.6	32.2
	1	235.3	195.8	140.1	113.5	80.1	59.2
	10	230.2	206	171.1	142.3	112.9	87.5
	100	259.6	208	177	159.4	120.2	83.8
0.3	0.001	145.8	97.1	63.7	36.4	18.8	8.1
	0.01	192.8	129	90.5	50.9	33.6	18
	0.1	211.3	156.6	114	74.2	53.7	28.6
	1	222.4	184.8	133	106.2	76.2	52.4
	10	219.5	196.5	162	133.1	106.6	77.9
	100	232.1	197.5	170	147.2	112.3	61.2
0.4	0.001	137.6	92.2	60.7	33.9	18.5	8.1
	0.01	178.7	126	87.5	50.1	31.7	18
	0.1	202	153.1	111.7	72.7	54.8	28.6
	1	199.1	176.4	126.4	100.7	73.7	52.4
	10	167.2	188.1	152.4	124.9	100.4	77.9
	100	241.3	190.4	159.2	132.8	106.4	61.2
0.5	0.001	132.2	89.9	57.5	32	17.4	8.4
	0.01	176.6	122.4	84.2	47.7	32.2	18
	0.1	200.8	150.1	107.1	69.3	42.6	26
	1	208.1	171.2	121.4	95.7	70.2	51.1
	10	193.2	182.2	144.8	119.2	95.5	74
	100	232.1	183.7	149.2	122.3	99.2	53.7

true strain, and their respective flow stress values at 0.1, 0.2, 0.3, 0.4, and 0.5 were tabulated as in Table 1. Since 2D maps can correspond to one strain value only, a minimum of five processing maps (for the five strains) would be needed, but the reader will not be able to connect optimum deformability ranges between one map to the next. On the other hand, in the 4D map, the efficiency and instability values are shown as a continuum in the entire deformation space, and can be viewed in a contiguous fashion.

Fundamental theory of processing maps

Processing maps are based on "Dynamic Materials Modeling" (DMM) [5–10], which are widely used to define the workability of materials. They are generated by the superimposition of power dissipation and instability maps and illustrate the visual response of the change in the microstructural characteristics of the material's response with respect to the change in hot working conditions. Material modeling based on its dynamic nature is important to define the material processing parameter for preferable deformation at elevated temperatures, which in turn defines the flow behavior of the work piece under study.

Deformation parameters

Dynamic recrystallization

Dynamic recrystallization (DRX) is a thermally activated process which occurs when a critical level of strain energy is achieved. Thus, a high level deformation stimulated by the nucleation and growth process is required in this process to govern the plastic flow behavior that also affects the microstructural characteristics of a thermo-mechanically processed metal or alloy. DRX provides stable flow and good workability to the material by simultaneous softening, and a power relationship exists between the dynamically recrystallized grain size and the peak stress.

Dynamic recovery

Dynamic recovery (DRY) occurs at elevated temperatures and high strain rates. The reason for these conditions is the availability of sufficient atomic mobility in response to the local stress to balance the work hardening. New grains are evolved and accelerated by the dense dislocation walls evolved in the original grains through the development of serrated grain boundaries and strain-induced dislocation sub-boundaries. Recovery minimizes the effect of work hardening by allowing the atomic rearrangement to reduce the internal stress arising within the grain.

Theoretical background of innovation

Strain independent power law [11]

This fundamental equation provides a direct dependency of flow stress with strain rate. According to this law, the flow behavior of a material under uniform plastic deformation can be expressed by the simple power relation,

$$\sigma(\varepsilon, T) = k\dot{\varepsilon}^m \quad (1)$$

k is constant for a particular strain, strain rate, and temperature. The exponent "m" is also constant at a given strain and temperature and is generally referred to as "strain rate sensitivity parameter" whose value always lies between 0 and 1. Mathematically "m" is determined by the slope of the plot of ln (σ) versus ln ($\dot{\varepsilon}$).Thus,

$$m = \frac{\mathrm{d}(\ln \sigma)}{\mathrm{d}(\ln \dot{\varepsilon})} \tag{2}$$

Determination of power dissipation using dynamic material modeling

The power dissipated in a particular deformation process is the rate at which work is performed or the amount of energy transmitted for a given unit of time. According to DMM, the power P (per unit volume) absorbed by the work piece with plastic flow at any strain and temperature is expressed in terms of two complementary functions, G (the dissipater content) and J (the dissipater co-content).

$$P = G + J \tag{3}$$

G and J are taken from the basic principle of thermodynamics; G represents the dissipation of power by the plastic work, and J the part of the work that occurs during the dynamic metallurgical deformation. All the plastic instabilities are associated with the G content, whereas the microstructural evolution is associated with J co-content.

According to dynamics, the work is related to the load (F) and the stroke (ΔS) acting on it,

$$W = F \cdot \Delta S \tag{4}$$

In this way, the net instantaneous equivalent power required by the work piece in the whole deformation range of the sample of unit cross section area and unit gauge length is given by

$$\bar{P} = \bar{\sigma}(t) \cdot \dot{\bar{\varepsilon}}(t). \tag{5}$$

Clearly, the average power dissipated in a thermo-mechanical deformation process at a particular strain and temperature is the area of the rectangle in the whole strain rate range when the flow stress and strain rate are taken along the two coordinate axes. Figure 1 shows an example

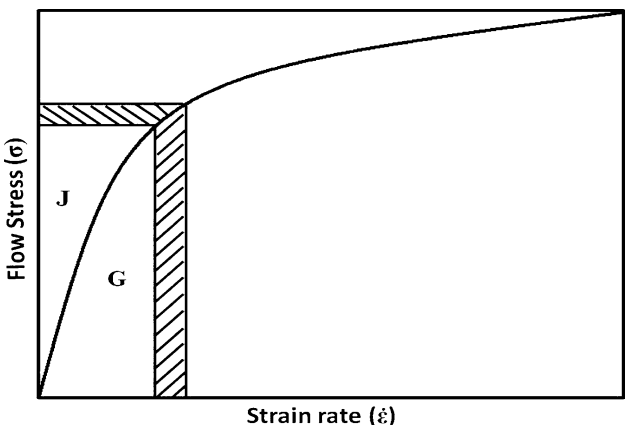

Fig. 1 Flow stress–strain rate curve representing G and J content

flow stress–strain rate diagram where the areas separated by the curve consist of two parts due to the mechanical behavior of the material being processed:

1. The first area is above the equivalent flow stress curve, which represents the J content of the plastic work. The flow stress in this area is characterized by the function of $\varepsilon, \dot{\varepsilon}$ and T:

$$\sigma = f_1(\varepsilon, \dot{\varepsilon}, T) \tag{6}$$

2. The second area is below the equivalent flow stress curve and represents the G content of the plastic work. The constitutive equation characterizing the strain rate in this part is a different function given as:

$$\dot{\varepsilon} = f_2(\sigma, \varepsilon, T) \tag{7}$$

In lieu of these equations, the net instantaneous equivalent power in the underlying deformation process is represented as the sum of two definite integrals corresponding to the assigned response of the material being tested:

$$\bar{P} = \int_0^{\dot{\bar{\varepsilon}}} f_1 \mathrm{d}\dot{\varepsilon} + \int_0^{\bar{\sigma}} \dot{\varepsilon} f_2 \mathrm{d}\sigma \tag{8}$$

The first integral in Eq. 8 corresponds to the G content of the plastic deformation, whereas the second represents the J co-content of the same deformation. The strip shown in Fig. 1 represents the small cross section of the area defining the above integrals.

Process efficiency of power dissipation

The DMM is used to analyze the deformation of metals in the high temperature regime. Assuming that the flow stress is well represented by a power law, the G and J contents will be respectively defined as follows [12]:

$$G = \frac{\bar{P}}{1+m} \tag{9}$$

$$J = \frac{m\bar{P}}{1+m} \tag{10}$$

In modeling the dynamic material behavior, a non-dimensional efficiency index η is used to represent the power dissipation and is called the power dissipation efficiency index. This index is the ratio of the J value to its maximum value, which directly depends on the m value of the power law. In lieu of Eq. 2, the maximum value of J will be obtained at unit value of strain rate sensitivity,

$$J_{\max} = \frac{\bar{P}}{2} \tag{11}$$

Thus, the efficiency of power dissipation is given as [4–9]

$$\eta = \frac{2m}{m+1}. \tag{12}$$

It is noted that the efficiency of power dissipation (η) derived from G and J is used for maximizing the efficiency of the process and for the analysis of instability in metal forming a wide range of materials. The temperature and strain rate corresponding to the peak efficiency region are generally selected to optimize this parameter.

Instability of processing maps

According to Ziegler's criterion of instability regions in process maps [13], the flow instability in these maps occurs when the dynamic metallurgical deformation function $D(\dot{\varepsilon})$ follows the following condition

$$\frac{dD}{d\dot{\varepsilon}} < \frac{D}{\dot{\varepsilon}} \tag{13}$$

In accordance with the dynamic material model, the dynamic metallurgical deformation function is equivalent to the J content, which represents the power dissipation occurring through microstructural changes.

As the dissipation characteristics vary for different microstructural mechanisms, each domain on the map can be correlated to a single dominant mechanism operating under the same condition of the domain. For this reason, processing maps are also referred to as power dissipation maps. The instability criterion is given by the following equation [4–9]

$$\Sigma(\xi) = \left\{ \frac{\partial \ln\{m/(m+1)\}}{\partial \ln \dot{\varepsilon}} \right\} + m \leq 0 \tag{14}$$

This equation is applied to delineate the temperature–strain rate regimes of flow instability on the process map. Flow instability generally occurs at high strain rates where the heat generated due to an increase in local temperature as a result of plastic deformation is not conducted away to the cooler regions of the body. Since the time available is short, cracking, recrystallization, and phase transformation occur along the macroscopic shear planes due to Adiabatic Shear Bands (ASBs) [4]. This is one of the reasons for the occurrence of flow instability in these materials. In this region, the net entropy change in the material system is not proportional to the input entropy.

Experimental procedure

Thirty six uni-axial compression tests were carried out using cylindrical samples 15-mm high and 10-mm diameter fabricated from as cast Al 2024 alloy billet of diameter 70 mm. The top and bottom faces of the specimens were machined parallel and had concentric grooves 0.5-mm deep to retain the lubricant (MoS_2) during compression and to reduce the friction of the die–workpiece interface. The deformation tests were carried out with a 50 kN computer-controlled BiSS ® servo-hydraulic UTM equipped with an ATS® three zone split furnace. To obtain a constant true strain rate value, the ram was instantly automatically corrected at each strain value to account for the change in strain at very small intervals using the following equation

$$X(t) = h_0[1 - \exp(\dot{\varepsilon}t)] \tag{15}$$

where, $X(t)$ is the stroke at the time "t", h_0 is the initial height of the specimen, and $\dot{\varepsilon}$ is the true strain rate.

The load-stroke data obtained by the tests were then converted to true stress–strain data using the following equations which further were used to generate the processing maps and the 4D maps.

$$\text{True strain } (\varepsilon) = \ln[h_1/h_0] = \ln(e+1)$$

$$\text{True stress } (\sigma) = p/[A_0(e+1)]$$

where, p = load, h_0 = original height, h_1 = change in length at any instant of time, e = engineering strain, and A_0 = original area of the sample.

From the true stress–strain data, flow stress values are tabulated, and these values are used for calculating efficiency (η) and instability (ξ). A processing map is generated based on the calculated efficiency and instability values at each strain. Since a minimum of five processing maps have to be generated for understanding the complete deformation behavior of the particular alloy, which is a tedious job, a new hybrid 4D map is generated for easier representation of the entire deformation behavior with one rendering.

The temperature range chosen for the compression tests were 250–500 °C for strain rates between 10^{-3} and 10^{2} s^{-1}. All the specimens were deformed by 50% (corresponding to a true strain of 0.67), and the flow stress curves were obtained for each of the tests. The specimens were cut in the transverse direction and cold mounted, polished, and etched with Keller's reagent for microstructural observations with a Leica® optical microscope.

Results and discussion

True stress–strain curves

Flow curves representing the material's behavior for the entire strain range at two working temperatures of 350 and 500 °C are shown in Fig. 2. At temperatures less than

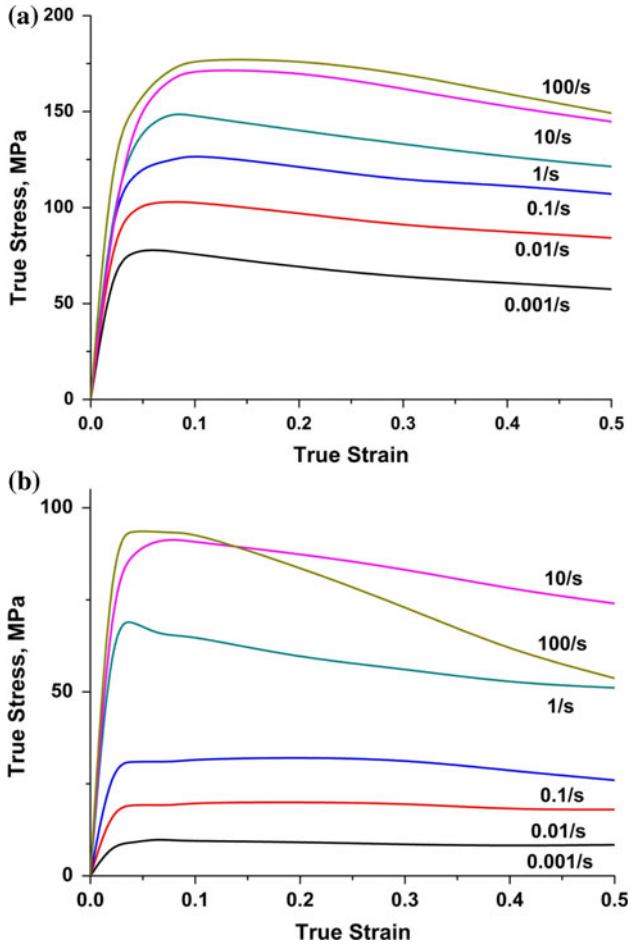

Fig. 2 **a** Flow stress curves at 350 °C at different strain rates. **b** Flow stress curves at 500 °C at different strain rates

350 °C, the material exhibits severe work hardening followed by continuous flow softening. Flow softening is a common characteristic of true stress–strain curves for many alloys deformed at elevated temperatures. It can be caused by deformation heating that creates microstructural instabilities such as DRX, texture formation, dynamic precipitation, and dissolution inside the material. In this case, the flow softening seems to be more pronounced at low strain rates that indicate the role of microstructural instability. At higher temperatures (>350 °C), the flow behavior is distinctly different. At these temperatures, the initial work hardening component is reduced, and the material exhibits only steady-state flow behavior at strain rates less than $\leq 10^{-1}$ s^{-1}, while at higher strain rates, work hardening is restricted to smaller strains followed by mild flow softening leading to steady-state flow.

It is evident from the figures that at high strain rates (10^{1} and 10^{2} s^{-1}) there is no prominent change in flow stress, and the peak stress increases with an increase in strain rate and decreases with increasing deformation temperature. The curve shown in Fig. 2b corresponds to a strain rate of 10^{2} s^{-1} and shows a predominant lowering in the slope due to dynamic work softening at a strain value of nearly 0.15 signifying the occurrence of the DRX mechanism.

Processing maps and microstructure evolution

Figure 3a, b, and c shows the processing maps for Al 2024 at true strains of 0.1, 0.3, and 0.5, respectively. The semi closed contours in the map represent percentage power dissipation efficiency, which in turn represents the relative rate of entropy production during deformation. The shaded domains indicate the region of flow instability (negative flow instability parameter), while the higher efficiency corresponds to microstructural changes due to DRX and DRY, which in turn represent effective processing conditions. The maximum efficiency in this case is found to be 46% at 500 °C and between 10^{-2} and 10^{-1} s^{-1} representing the low strain rate domain, also confirmed by the microstructure (Fig. 4c–f). The safe deformation zone is identified to be between 350 and 500 °C in the strain rate range of 10^{-3} to $10^{0}s^{-1}$, which is also supported by the microstructure in Fig. 4c–f. Another deformation zone is identified between 250 and 300 °C in the strain rate range of 10^{1} to 10^{2} s^{-1} representing the high strain rate domain. Since, this domain has lower efficiency; it is not considered suitable for processing. Dashed contours represent flow instability where the efficiency is negative corresponding, which corresponds to microstructural inabilities such as wedge cracking, slip, dislocation, etc.

Figure 4a corresponds to the as-cast Al 2024 microstructure, which is multi-phase and consists of fine soluble Al_2CuMg precipitates along with iron-rich phases. The microstructure of the specimen deformed at high temperatures and high strain rates indicate some amount of precipitation at the grain boundaries and a small amount of elongation of the grains corresponding to the initiation of DRX in the system. This is also evident from flow softening of the flow curves at these high temperatures and high strain rates. Elongated grains with serrations were observed at grain boundaries, which provide additional evidence that DRX is occurring during hot compression deformation, and that the DRX grain size is strongly dependent on deformation temperature and/or strain rate. With increasing strain, the grains became thinner and the serrations in opposite elongated boundaries came into contact indicating shortening of the grains leading essentially to grain refinement. The solutes and a uniform dispersion of fine particles interact with the dislocations to reduce DRY, which leads to the higher stored strain energy probably speeding up DRX during hot deformation. This DRX process, resulting from the DRY mechanism, leads to

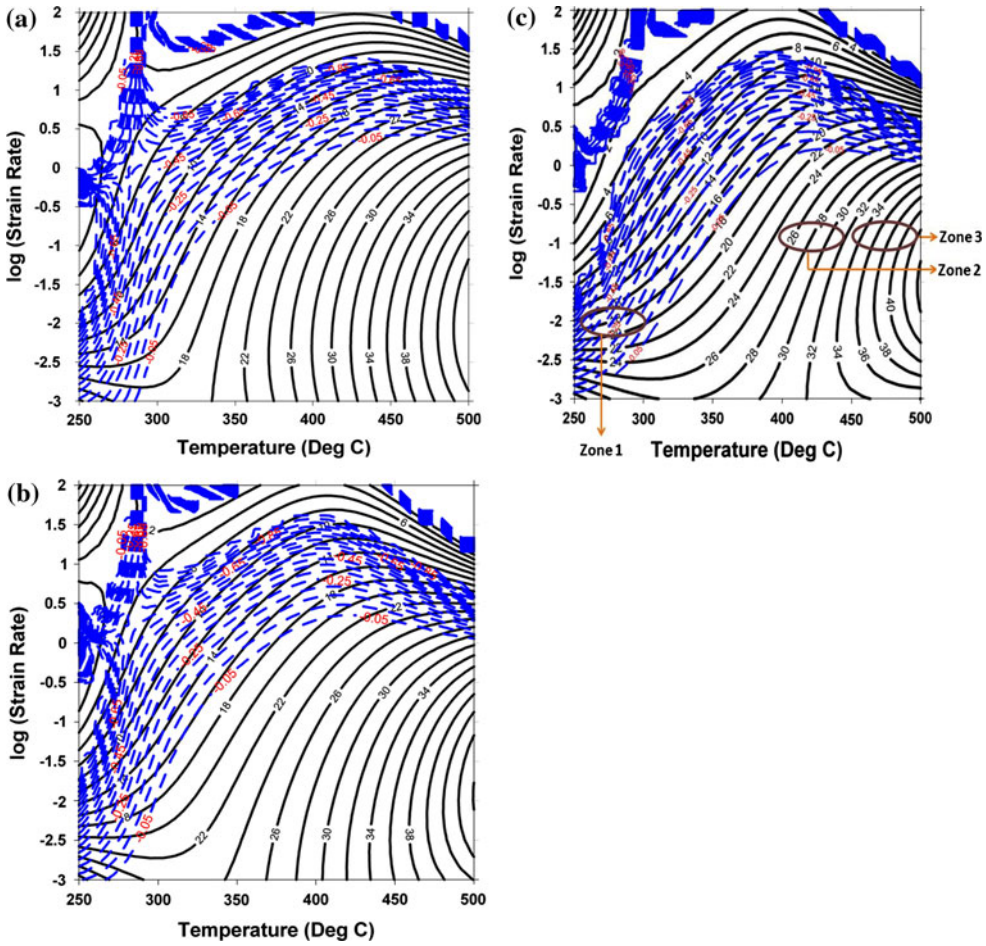

Fig. 3 **a** Processing map at a true strain of 0.1. **b** Processing map at a true strain of 0.3. **c** Processing map at a true strain of 0.5

grain refinement, and it is proposed that this be referred to as geometric dynamic recrystallization (GDRX).

Figure 4c–f shows the deformed microstructure at 400 °C at 10^{-1} s^{-1} and 500 °C at 10^{-1} s^{-1}, respectively. The DRY mechanism is apparent in Fig. 4c and d, corresponding to zone 2 of the processing map and the 4D Power dissipation map (Fig. 5a). The observation of sub-grains and their precipitation at grain boundaries, as shown in Fig. 4e and f, signifies the DRX mechanism in the third zone of the processing map and 4D Power dissipation map (Fig. 5a). It is found that as the strain rate increases, finer structures with a large number of sub-grains have formed. Figure 4b represents microstructural instability (flow localization) at 250 °C and 10^{-2} s^{-1} corresponding to zone 1 in processing map and 4D Instability map (Fig. 5b).

Benefit of the 4D process map

Previously, only hit and trial method is the only mean to obtain the best processing condition and control the microstructure of the particular metal or alloy. However, as a result of lack in continuity of the observation of processing parameters, the hit and trial method may sometimes be unable to reach the best suitable condition. Thus, it is necessary to link the processing model to some material's visual continuum model that depicts the continuity in deformation parameters. Process map is the outcome of the continuum model which is based on FEM simulation that forms a link between different deformation stages and helps in optimizing the processing parameters from the point of view of hot workability and control of microstructure. It was suggested earlier that process maps at different strains do not show much difference and the strain components only define the frame of the microsystem [14]. DMM forms the basis of this microstructural modeling. According to which, the flow stress increases with strain in the initial deformation and reaches a constant value for metals exhibiting DRY. On the other hand, when DRX occurs, the flow stress instead increases with increasing strain and attains a maximum value, after which the stress decreases, eventually attaining a steady-state value. In general, the flow stress varies greatly with strain [15–19]. The visual process modeling is also important in showing the effect of stress and strain that particularly

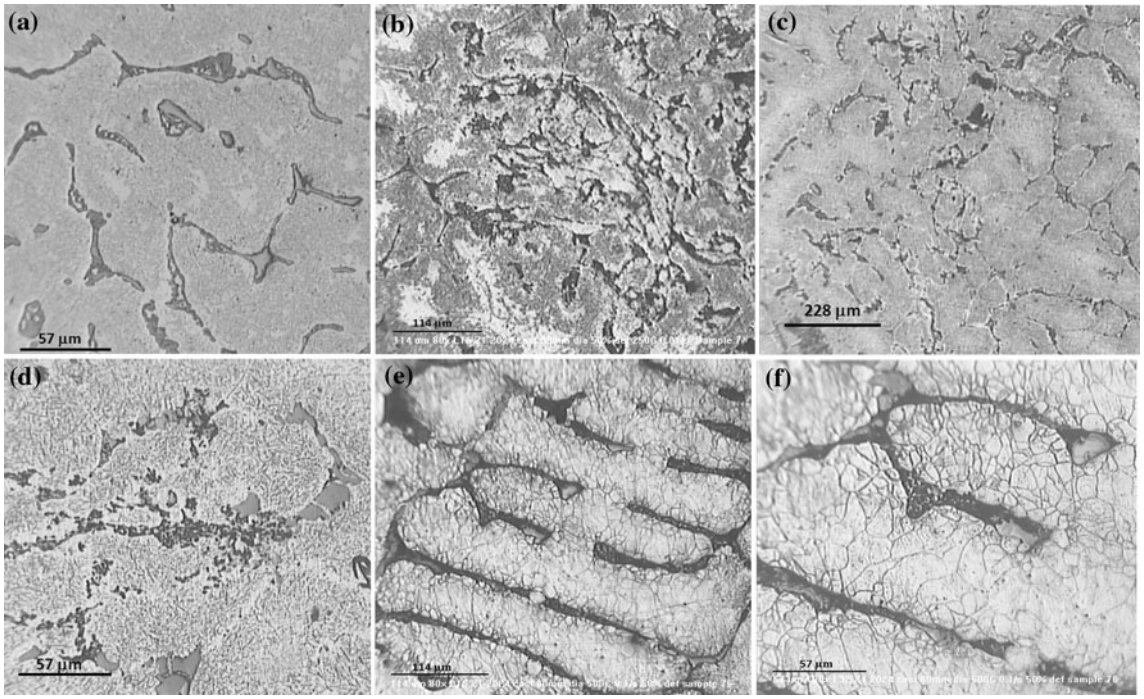

Fig. 4 **a** As cast microstructure. **b** Flow localization at 250 °C at 10^{-2} s^{-1}. **c** DRY mechanism observed at 400 °C at 10^{-1} s^{-1} at lower magnification. **d** DRY mechanism at 400 °C at 10^{-1} s^{-1} at higher magnification. **e** DRX mechanism observed at 500 °C at 10^{-1} s^{-1} at lower magnification. **f** Sub grain formation due to DRX at 500 °C at 10^{-1} s^{-1} at higher magnification

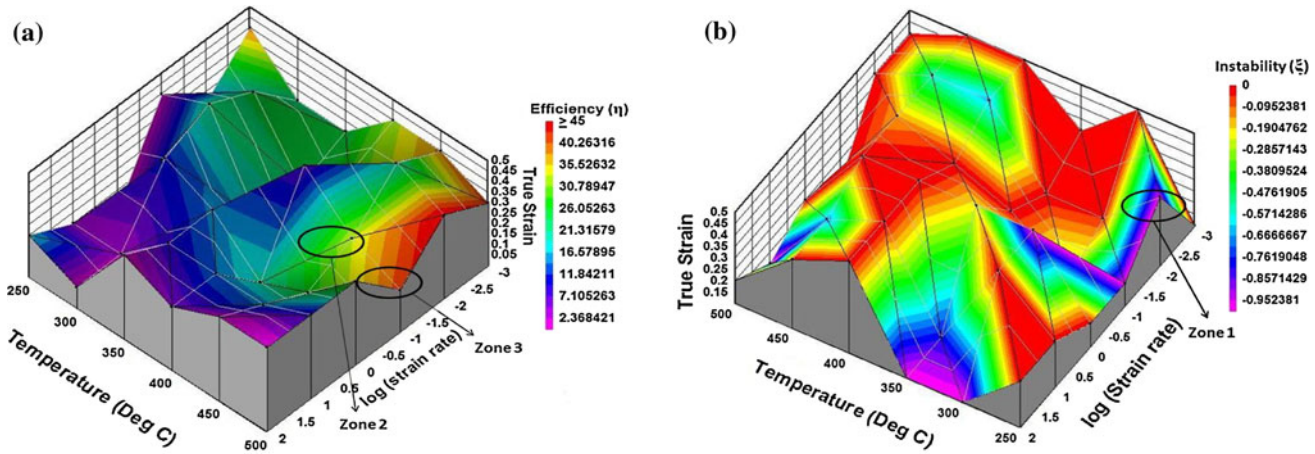

Fig. 5 **a** 4D Power dissipation map. **b** 4D Instability map

helps in designing the elevated temperature working processes, as well as for solving the problems encountered in every metal working practice.

Conventional process map is a two dimensional entity of the process carried out in lieu of the deformation experiments. It does not involve the variation of strain, since the maps are generally presented at a constant strain. So, in these 2D maps, one of the processing variables, i.e., true strain is kept constant to a particular value, whereas the remaining variables provide the graphical representation. This is the reason for the necessity of the constellations of maps for the complete simulation of the deformability. Liu et al. have made an effort to overcome this drawback and generate the 3D processing map [20]. However, these maps also do not show the variation of strain in an integrated manner, as they are basically the stacking of process maps over each other at different strains. In order to enhance the representation of all the process variables in same graph, another medium of representation is required. The present 4D map fulfills the long ever requirement of continuum

deformation mechanics. The feasibility of the fourth dimension is made by giving the color code to the three dimensional graph. This multidimensional visualization is capable to capsulate all the numerical information under the same scale. Based on the algorithm of 2D process map, an attempt has been made in this article to generate a new hybrid 4D process map that illustrates power dissipation η and instability ξ with a variation in strain rate, temperature, and strain. These maps were generated using DPLOT® graphing software. Efficiency (η) and instability (ξ) were calculated with software developed in our lab and this was, in turn, used to generate the 2D and 4D process maps. To avoid the duplicate values of x and y with respect to the z frame of reference, this graphing software chooses the unique values of x and y from the set of analytic data. This in turn ensures the best possible clarity in the map and helps one to visualize the complete deformation behavior of the work pieces in a glance. Simulation and analytical results show that the use of this multidimensional mapping can significantly help in improving system performance. However, there is a need to develop graphing softwares by which we can see a sliced view of the 4D process map at any parameter for assessing deformation efficiency and potential for instability for any process condition.

Figure 5a represents a 4D power dissipation map in which log(strain rate), temperature, and strain are plotted on x, y, and z axes, respectively, with efficiency (η) as amplitude. This map visualizes the entire deformation space in one view. Two safe deformation zones were also identified in the 4D map. However, in comparison to the 2D maps, the 4D map in addition also shows the strain space over which this efficiency prevails. The first zone lies in a true strain range between 0.2 and 0.5 for strain rates between 10^{-3} and 10^{0} s^{-1}, for temperatures between 350 and 500 °C corresponding to an efficiency of 36–46%. This would correspond to zones 2 and 3 in the 2D process maps. Figure 5b represents a 4D instability map in which log (strain rate), temperature, and strain are plotted on the x, y, and z axes, respectively, and the instability (ξ) is the amplitude (4D). The thick color indicates the highest instability which confirms the microstructure observations of wedge cracking, flow localization, void formation, etc. This same zone is identified as zone 1 in the process map, but is seen in strain space in the 4D map.

Conclusion

Hot compression tests of 2024 aluminum alloy were performed in the temperature range from 250 to 500 °C at strain rates between 10^{-3} and 10^{2} s^{-1}. The associated microstructural changes were studied with light microscopy, and 2D and 4D processing maps were generated. The following was concluded:

(1) The true stress–true strain curves exhibit a peak stress at a critical strain, after which the flow stress decreases monotonically until high strains, showing dynamic flow softening. The peak stress decreases with increasing deformation temperature and decreasing strain rate.
(2) The microstructure of the specimen deformed at high temperatures at high strain rates indicates some amount of precipitation at the grain boundaries and a small amount of elongation of the grains corresponding to the initiation of DRX in the system. This is the main cause for flow softening.
(3) The 2D and 4D processing maps exhibit two domains as optimum fields for hot deformation at different strains: the low strain rate domain at 500 °C between 10^{-2} and 10^{-1} s^{-1} and a high strain rate domain between 250 and 300 °C in the strain rate range of 10^{1} to 10^{2} s^{-1}.
(4) The 4D process map, which is now possible with advancements in software, is a better representation of complete deformation behavior compared with the conventional 2D process map, since the latter does not show the variation of efficiency and instability with strain.

Acknowledgements The authors are thankful to the Director, AMPRI, Bhopal for granting the permission to publish this article, Prof. V. Rao for helping in revising the technical content of the article. The authors are also thankful to the reviewers for their invaluable comments and suggestions, without which the article may not be in the present form.

References

1. Malas JC, Venugopal S, Seshacharyulu T (2004) Mater Sci Eng A 368:41
2. Babu NS, Tiwari SB, Nageswararao B (2005) Mater Sci Technol 21(8):976
3. Sellars CM, Zhu Q (2000) Mater Sci Eng A 280:1
4. Maheshwari AK, Pathak KK, Ramakrishnan N, Narayan SP (2009) J Mater Sci 45(4):859. doi: 10.1007/s10853-009-4010-x
5. Prasad YVRK, Sasidhara S (1997) Hot working guide: A compendium of processing maps. ASM International, Metals Park
6. Sivakesavam O, Rao IS, Prasad YVRK (1993) Mater Sci Technol 9:805
7. Prasad YVRK, Giegel HL, Doraivelu SM, Malas JC, Morgan JT, Lark KA, Barker DR (1984) Metall Mater Trans A 15:1883
8. Srinivasan N, Prasad YVRK, Rama Rao P (2008) Mater Sci Eng A 476:146
9. Siva Prasad PV, Venu Gopal S (2003) J Mater Eng Perform 12(6):656
10. Ravichandran N (2003) J Mater Eng Perform 12(6):653
11. Campbell FC (2008) Elements of Metallurgy and Engineering Alloys. ASM International, Metals Park

12. Narayana murty SVS, Nageswara rao B (1998) J Mater Sci Lett 17(14):1203
13. Narayana murty SVS, Nageswara rao B (1999) J Mater Sci Lett 18(21):1757
14. Sivakesavam O, Prasad YVRK (2003) Mater Sci Eng A 362:118
15. Jonas JJ, Sellars CM, Tegart WJMcG (1969) Met Rev 14:1
16. Sellars CM, Tegart WJ, Mc G (1972) Int Metall Rev 17(158):1
17. Glover G, Sellars CM (1973) Metall Mater Trans B 4(3):765
18. McQueen HJ, Ryan ND (2002) Mater Sci Eng A 322:43
19. Sellars CM (1978) Philos Trans R Soc 288:147
20. Liu J, Cui Z, Li C (2008) J Mater Proc Technol 205(1–3):497